

Spectral Fingerprint of Excited-State Energy Transfer in Dendrimers through Polarization-Sensitive Transient-Absorption Pump–Probe Signals: On-the-Fly Nonadiabatic Dynamics Simulations

Deping Hu, Jiawei Peng, Lipeng Chen, Maxim F. Gelin, and Zhenggang Lan*



Cite This: *J. Phys. Chem. Lett.* 2021, 12, 9710–9719



Read Online

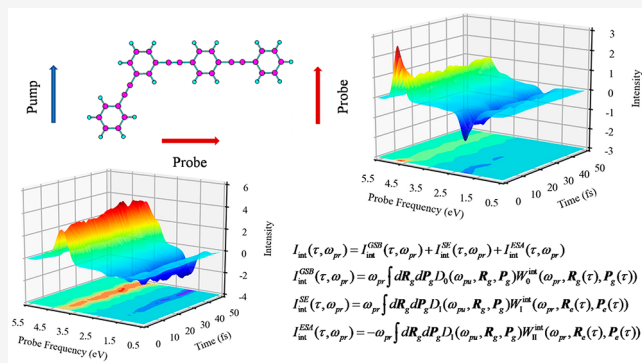
ACCESS |

Metrics & More

Article Recommendations

Supporting Information

ABSTRACT: The time-resolved polarization-sensitive transient-absorption (TA) pump–probe (PP) spectra are simulated using on-the-fly surface-hopping nonadiabatic dynamics and the doorway–window representation of nonlinear spectroscopy. A dendrimer model system composed of two linear phenylene ethynylene units (2-ring and 3-ring) is taken as an example. The ground-state bleach (GSB), stimulated emission (SE), and excited-state absorption (ESA) contributions as well as the total TA PP signals are obtained and carefully analyzed. It is shown that intramolecular excited-state energy transfer from the 2-ring unit to the 3-ring unit can be conveniently identified by employing pump and probe pulses with different polarizations. Our results demonstrate that time-resolved polarization-sensitive TA PP signals provide a powerful tool for the elucidation of excited-state energy-transfer pathways, notably in molecular systems possessing several optically bright nonadiabatically coupled electronic states with different orientations of transition dipole moments.



Downloaded via UNIV OF ROCHESTER on September 30, 2021 at 15:13:15 (UTC).
See https://pubs.acs.org/sharingguidelines for options on how to legitimately share published articles.

The dendrimer compounds comprising different phenylene ethynylene (PE) branches^{1–5} display excellent photoharvesting and exciton-transport properties. Therefore, they received considerable research interest owing to their potential applications in solar energy conversions.^{6–9} As each branch shows a different length, the electronic excited states of PE-based dendrimers are localized at each PE unit, and the energy of the local excited (LE) state localized at the short-length unit should be higher than that at the long-length unit. Under radiation fields, the LE states resonant to the radiative frequency are excited, and then the efficient unidirectional energy transfer should occur from the short-length units to the long-length units. Such systems represent ideal prototypes in the study of intramolecular excited-state energy transfer.^{2–5,7,8,10–15}

In dendrimer systems, the addition of the high conjugated units such as ethynylperylene groups does not modify the high-energy absorption band relevant to the LE state of the short PE units, while the efficient excited-state energy transfers take place after excitation. As a result, the LE state located at the larger PE units is formed, which gives the fluorescence emission.¹⁶ Several time-resolved spectroscopic studies suggested that the ultrafast energy migration takes place from the short-length PE units to the long-length PE units.^{4,17} Kleiman and co-workers confirmed the existence of LE states and the occurrence of further excited-state energy transfer in conjugated dendrimer systems.^{4,17}

Several pioneering works by Tretiak, Mukamel, and co-workers discussed the exciton transfer in PE dendrimers.⁶ These works included the possible control of the energy funneling to the desired site,¹⁸ the interplay between the entropic driving force toward the periphery and the energy gradient toward the center,¹⁰ etc. The essential role of exciton coupling in the exciton funneling process was clarified by the pump–probe (PP) spectra of dendrimer nanostars, which were simulated with the exciton motion and the doorway–window (DW) formalism.⁵ In fact, the energy-transfer processes in PE involve both electronic and nuclear motions. Roitberg, Shalashilin, Fernandez-Alberti, Tretiak, and co-workers performed a series of on-the-fly nonadiabatic molecular dynamics simulations with surface hopping and multiconfigurational Ehrenfest approaches at the semiempirical AM1/CIS level to study the intramolecular energy transfer in dendrimer systems.^{7,11,14} (see also ref 9 for a recent review). Fluorescence anisotropy kinetics were also simulated with rather simplified theoretical assumptions.^{15,19} Their works clearly demonstrated that the low-lying excited states mainly correspond to the

Received: August 11, 2021

Accepted: September 21, 2021



ACS Publications

different LE states at the Franck–Condon (FC) region, and ultrafast nonadiabatic transitions between different excited states finally result in the efficient unidirectional intramolecular energy transfer from the short-length conjugated branching subunit to the long-length one. For instance, the exciton motion from the 2-ring to 3-ring units takes place within 40 fs.

If the time-resolved spectra can be simulated by the combination of nonlinear response theories and on-the-fly nonadiabatic dynamics, we can obtain a more comprehensive understanding of the intramolecular energy-transfer dynamics of the PE dendrimers. For instance, we can directly establish the connections between spectroscopic signals and the coupled electronic–nuclear motions. However, the simulation of the time-resolved spectra on the basis of the on-the-fly nonadiabatic dynamics itself represents a challenging task. That is why simulations of such spectra with classical trajectories are rather limited, notably in comparison with a large number of simulations of population dynamics of molecular electronic states. In the following, we summarize the key results (see also ref 20 for a recent review). Mitrić, Bonačić-Koutecký, Martínez, and co-workers pioneered ab initio classical trajectory simulations of time-resolved photoelectron spectra.^{21,22} Time- and frequency-resolved fluorescence spectra were simulated by associating emission rates with the Einstein coefficient and invoking the classical Condon approximation.^{23–28} On-the-fly simulations of transient absorption (TA) PP spectra were performed by using different levels of ab initio theory and applying different theoretical methodologies.^{20,29–37} Garavelli, Mukamel, Nenov, and co-workers developed powerful protocols for on-the-fly simulations of TA PP signals of polyatomic chromophores by employing the cumulant/harmonic approximation for the evaluation of vibrational contributions and simulated TA PP spectra of rhodopsin,²⁹ trans-azobenzene,³⁰ thiouracil,³¹ and pyrene.³² Vaníček and co-workers have developed methodologies that approximate nonadiabatic electron-vibrational dynamics by using the multiple-surface dephasing representation³⁶ as well as constructing an efficient computational scheme based on the single Gaussian-wavepacket Ansatz.³⁷ Real-time time-dependent density-functional theory (RT-TDDFT) methodology³⁸ was also applied to the simulation of TA PP signals of several polyatomic molecules.^{33–35}

Recently, Gelin, Domcke, and co-workers proposed a practical approach for the on-the-fly trajectory simulation of TA PP signals which is based on the quasi-classical approximation of the DW representation of nonlinear spectroscopy.³⁹ The DW representation has been introduced into femtosecond spectroscopy by Yan, Fried, and Mukamel.^{40–42} For well-separated pump and probe pulses (non-overlapping pulses), the DW representation provides a transparent understanding of the TA PP signals. The interaction between the pump/probe pulse and the system is described by the doorway/window operator. Between the pump and probe pulses, the dynamics evolution is fully governed by the field-free system Hamiltonian. The TA PP signal is obtained by averaging the product of the doorway operator (at the time moment zero) and the window operator (at the time delay between the pulses) over nuclear trajectories generated by the surface hopping or other protocol for the on-the-fly simulation of the nonadiabatic dynamics. This DW representation does not add too much additional effort to the on-the-fly nonadiabatic simulations. Furthermore, this approach provides a clear and direct correlation between the

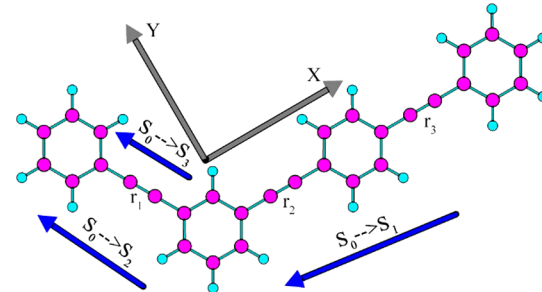
coupled electronic–nuclear motions in the energy-transfer process and the time-resolved spectroscopic response.

In this work, we extended the DW representation of ref 39 to account for polarization-sensitive detection of TA PP signals and combined it with the surface-hopping machinery for the on-the-fly simulation of TA PP spectra of PE dendrimers.

Polarization-sensitive detection schemes are commonly used in nonlinear femtosecond spectroscopy.^{43,44} If spectroscopic interrogation of the material system involves several transition dipole moments (TDMs) having different orientations in the system reference frame, polarization-sensitive detection permits one to dissect a four-wave-mixing signal into three different components and thus obtain more information on the system dynamics. In practical terms, it also enables the enhancement of desired (or suppression of unwanted) spectroscopic contributions.^{45,46} Notice that polarization-sensitive TA PP measurements were also performed on dendrimers,^{19,47,48} but these studies were focused on the processes occurring on the time scales from hundreds of femtoseconds to a few picoseconds.

A typical model dendrimer composed of meta-linked 2-ring and 3-ring units (in Scheme 1) was taken as an example in the

Scheme 1. Geometrical Structure of the PE Dendrimer Model at S₀-min^a



^aThe blue arrows indicate the directions of the TDMs from S₀ to the three low-lying excited states. The gray arrows indicate the directions of the coordinate axes, with the Z-axis perpendicular to the molecular plane.

current work, which is also a well-established model to study the excited-state energy transfer in the dendrimer system with different PE units.^{11,13} The on-the-fly nonadiabatic dynamics with Tully's fewest switches surface hopping (FSSH)^{49–56} was performed at the linear-response time-dependent density-functional (LR-TDDFT) level on the PE dendrimer model. The system was put in different initial electronic states, including the ground and low-lying excited states. Then, a series of dynamics calculations were performed with different initial states. During the dynamics simulations, the electronic-state energies and TDMs between different electronic states were recorded. After that, the DW approach was used to simulate the TA PP spectra of the dendrimer model for different polarizations of pump and probe pulses. We have shown that polarization-sensitive detection of TA PP signals allows one to monitor the ultrafast (several tens of femtoseconds) intramolecular energy transfer and disentangle energy-transfer pathways in dendrimers.

All the dynamics calculations were performed with a developing version of the JADE-NAMD package.^{57,58} The Gaussian 16 package⁵⁹ was used in the optimization and frequency analysis. The JADE-NAMD package interfaced with

the Qchem 5.1 package⁶⁰ was developed to perform the TDDFT calculations in the on-the-fly nonadiabatic dynamics. Here the analytical nonadiabatic coupling vectors at the TDDFT level^{61,62} were obtained directly instead of the numerical calculations of the time-derivatives of the wave function overlaps. All components of the TA PP signals, including the ground-state bleach (GSB), stimulated emission (SE) and excited-state absorption (ESA), were calculated within the quasi-classical approximation of the DW representation for femtosecond spectroscopy. More detailed discussions on the Hamiltonian, nonlinear response theories, DW representation, quasiclassical approximation, on-the-fly surface-hopping simulation are given in the Supporting Information.

The geometrical structure of S₀-min is shown in Scheme 1. The PE dendrimer model studied in this work is composed of 2-ring and 3-ring PE units, which is a prototype dendrimer model.^{11,13} For each unit, the benzene rings are linked with ethynylene bonds, whose distances are labeled as r₁, r₂, and r₃ in sequence from left to right in Scheme 1. The molecule is planar at S₀-min. To further discuss the polarized TA PP signals in this paper, the coordinate axes were set up. The X-axis is parallel to the 3-ring unit; the Y-axis is perpendicular to the X-axis and lies within the molecular plane; the Z-axis is placed perpendicular to the molecular plane.

The excited states at S₀-min were calculated at the TDDFT/CAM-B3LYP level with the 6-31G basis set, as shown in Table 1. S₁ is mainly composed of the local excitation at the 3-ring

unit, while S₂ is composed of significant contributions of the local excitation configuration at the 2-ring unit and a weaker component of the charge-transfer (CT) excitation between 2-ring and 3-ring units, as shown in Table S1 and Figure S1 in the Supporting Information. S₃ is mainly assigned as a CT state, and the residual TDM here may be due to the existence of the orbital overlap at the middle benzene ring. Although the electronic transition of S₄ is localized at the 3-ring unit, the TDM is nearly zero because of orbital symmetry.

From the electronic-structure point of view, the unidirectional excited energy-transfer process can be viewed as follows. The short-wavelength excitation (~4.64 eV) leads to the formation of the S₂ state because of its nonvanishing TDM, which corresponds to the LE state located at the 2-ring unit at the FC region. At the same time, S₃ may be weakly populated by the excitation at a similar wavelength because of the weak oscillator strength and the vibronic-borrowing electronic transition. Then the ultrafast nonadiabatic dynamics takes place, and the system quickly goes back to S₁ dominated by the local excitation component at the 3-ring unit; that is, the ultrafast excited-state energy transfer occurs from the short-chain to long-chain units.

The directions of TDMs from the ground to the first three excited states are shown in Scheme 1. The direction of the TDM of S₁ is nearly aligned with two CC triple bonds of the 3-ring unit, while the directions of the TDMs of S₂ and S₃ are nearly along the CC triple bond of the 2-ring unit. This is consistent with the fact that S₁ and S₂ are mainly composed of the LE states located at the 3-ring and 2-ring units, respectively. No TDM component was observed along the Z-axis that is perpendicular to the molecular plane.

To analyze the TA PP signals more conveniently, we plotted the TDMs between different electronic states at S₀-min (see Figure 1). The TDM components in the X-axis and Y-axis directions are presented separately. The relation between the TDMs and signals is further discussed in the rest of this Letter.

To perform on-the-fly simulations of the TA PP signals and to facilitate interpretations of the obtained results, we have grouped the molecular states into three energetically well-

Table 1. Vertical Excitation Energies (VEEs) and TDMs of the Four Low-Lying Electronic States at the TDDFT/CAM-B3LYP/6-31G Level at S₀-min of PE Dendrimer Model

VEE (eV)	TDM (Debye)				
	X	Y	Z	tot	
S ₁	4.03	12.09	-1.36	0	12.17
S ₂	4.64	2.88	-5.97	0	6.63
S ₃	4.71	0.77	-1.41	0	1.61
S ₄	4.99	0	-0.09	0	0.09

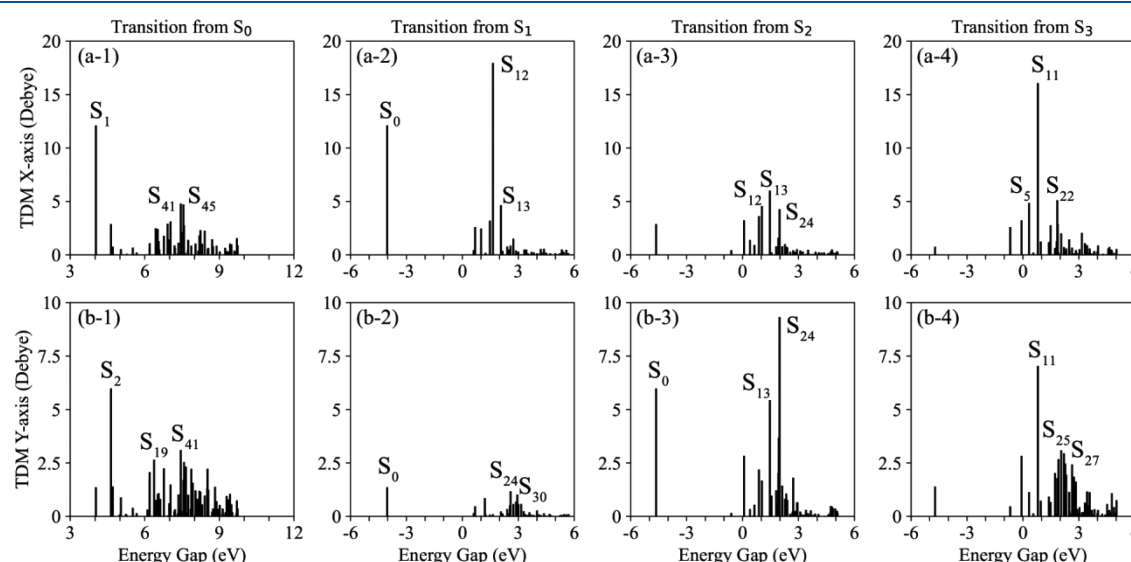


Figure 1. Absolute values of transition dipole moments (TDMs) in the (a) X-axis and (b) Y-axis direction from (1) S₀, (2) S₁, (3) S₂, and (4) S₃ to other electronic states at S₀-min. The three largest TDMs are labeled. 150 states are involved in the TDDFT calculations at the CAM-B3LYP/6-31G level.

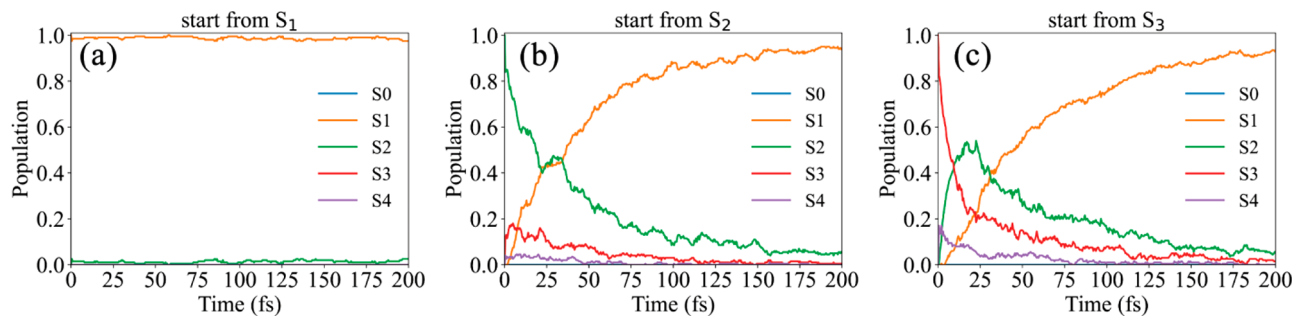


Figure 2. Time-dependent electronic populations of S_0 – S_4 in the on-the-fly surface hopping nonadiabatic dynamics, which start from (a) S_1 , (b) S_2 , and (c) S_3 . 200 trajectories were used for each initial state.

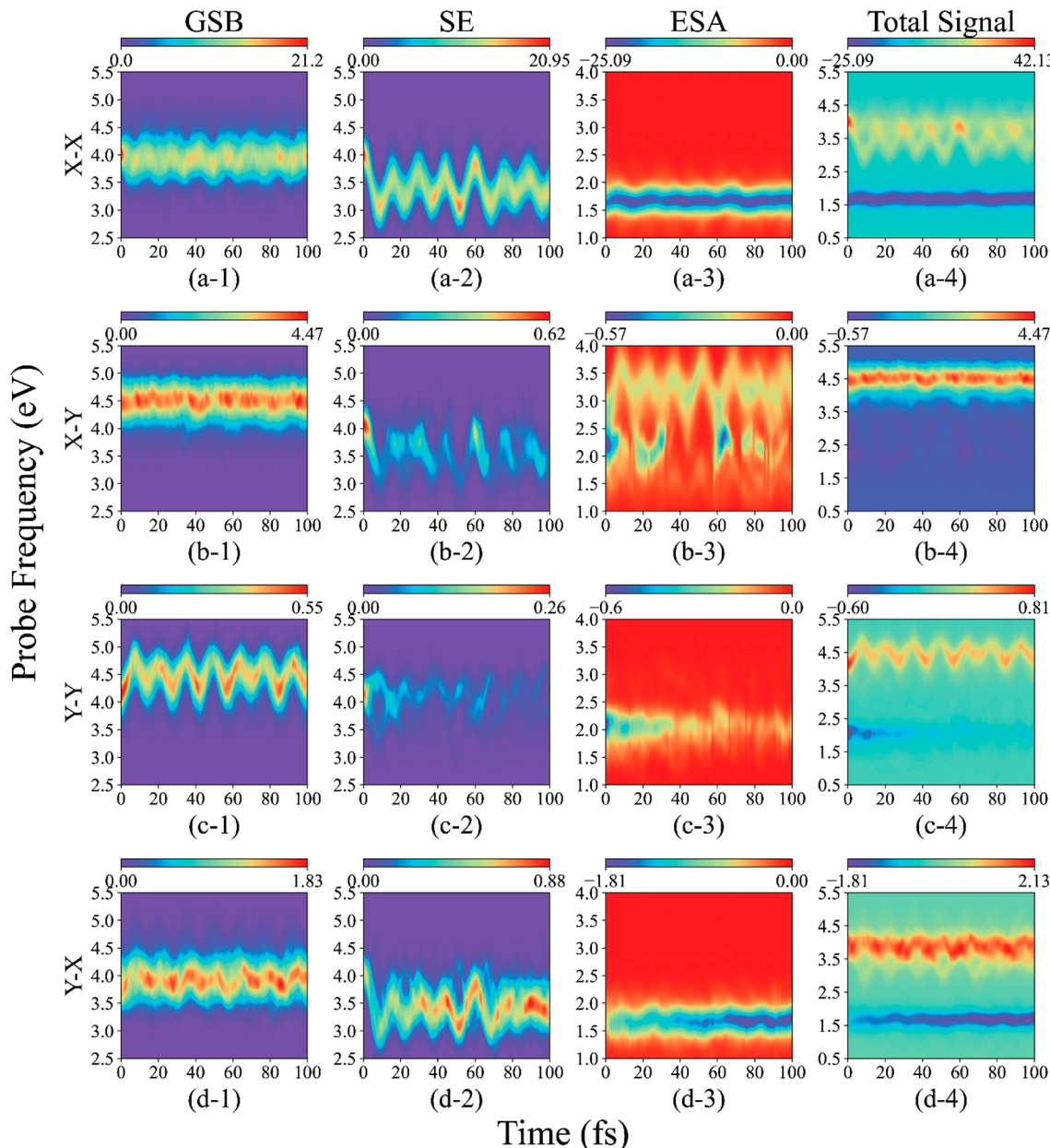


Figure 3. (1) GSB, (2) SE, and (3) ESA contributions and (4) total integral signal $I_{\text{int}}(\tau, \omega_{\text{pr}})$ as a function of τ and ω_{pr} . The notation $\alpha-\beta$ ($\alpha, \beta = X, Y$) on the left side indicates that the pump pulse polarization (ϵ_{pu}) is along the α -axis direction, while the probe pulse polarization (ϵ_{pr}) is along the β -axis direction. The central frequency of the pump pulse is $\omega_{\text{pu}} = 4.03$ eV, and the pulse durations are $\tau_{\text{pu}} = \tau_{\text{pr}} = 5$ fs.

separated manifolds {0}, {I} and {II}, where {0} is the electronic ground state; {I} comprises the states which can be

interrogated by the pump pulse from the electronic ground state as well as other states which are dynamically (non-

adiabatically) coupled to these states; {II} includes the states which can be interrogated by the probe pulse from the manifold {I}. In this work, the lowest four excited states (S_1 , S_2 , S_3 , and S_4) were included in manifold {I}, and the other 146 excited states with VEEs up to 10 eV were incorporated in manifold {II}.

The on-the-fly nonadiabatic dynamics simulations for the PE dendrimer model were performed assuming initial excitation in the states S_1 , S_2 , and S_3 . Excitation to S_4 was not considered because this state has a vanishing TDM. Nonadiabatic transitions among all 4 states of manifold {I} were allowed for completeness. The time-dependent electronic populations are shown in Figure 2.

When the initial state is S_1 (see Figure 2a), most trajectories stay at this state during the whole dynamics. When the initial state is S_2 (see Figure 2b), the system decays to S_1 rapidly. About a half of the trajectories decay to S_1 within 35 fs, and most trajectories decay to S_1 at the end of simulation time 200 fs. The higher excited states, S_3 and S_4 , are weakly populated in the early stage of dynamics. When the initial state is S_3 (see Figure 2c), the system first decays to S_2 very rapidly, and then S_1 is populated. Nearly half of the trajectories reach S_1 at 45 fs. Similar to the case when dynamics starts from S_2 , most of the trajectories decay to S_1 at the end of the simulation time.

The time-dependent electronic populations show that the system quickly decays to S_1 if the trajectories start from S_2 and S_3 , which agrees well with previous on-the-fly nonadiabatic simulations at the semiempirical level of theory.^{11,14,63} As presented before, S_1 is nearly an LE state at the 3-ring unit, and S_2 is a hybrid LE state at the 2-ring unit and CT state between the 2-ring and 3-ring units. The fast nonadiabatic decay from S_2 to S_1 leads to the ultrafast excited-state energy transfer from the short-conjugated unit to the long-conjugated unit. In addition, we also noticed that the S_1 and S_2 energy gap becomes very small at the long r_1 distance (Figure S2a-1), and thus, the r_1 stretching motion (Figure S3a-3) drives the nonadiabatic transition from S_2 to S_1 . This observation is also highly consistent with previous work.^{11,14,63}

The TA PP signals of the PE dendrimer model were simulated using the DW representation of nonlinear response as described in ref 39 and detailed in sections S1–S5 of the Supporting Information.

We assume that the PE dendrimers are aligned (e.g., by the incorporation into a matrix/film or by the application of an external field) in the reference frame of Scheme 1 and study 4 variants of the polarizations (ϵ_{pu} , ϵ_{pr}) of the pump and probe pulses along the axes X and Y: (X–X), (X–Y), (Y–Y), and (Y–X). Pump pulses with two different frequencies, $\omega_{pu} = 4.03$ and 4.64 eV resonant with S_1 and S_2 , were considered in the simulation. Notice that the energies of S_2 (4.64 eV) and S_3 (4.71 eV) are very close, so the S_3 contribution was also taken into account in the simulation. Below, we will give a detailed analysis of the integral TA PP signals. The dispersed signals contain the same information and are presented in the Supporting Information (Figures S4 and S5). In the simulation of TA PP signals, the pump and probe pulses with Gaussian envelopes were used, namely, $E_a(t) = \exp\{-(t/\tau_a)^2\}$ and $E_a(\omega) = \exp\{-(\omega\tau_a)^2/4\}$ ($a = pu, pr$). As is well-known, the time-frequency resolution of integral TA PP signals is Fourier-limited (see ref 64 for the detailed discussion). For the simulation of these signals, the pulse durations τ_a are set to 5 fs, which yields the bandwidth of 0.44 eV (full width at half-maximum). On the one hand, such ultrashort pulses are not

uncommon in spectroscopic laboratories. On the other hand, 5 fs pulses allow us to monitor fast vibrational wavepacket oscillations, and their bandwidth of ~0.44 eV is sufficient for covering all spectral features in $I_{int}(\tau, \omega_{pr})$. The time-frequency resolution of dispersed TA PP signals is not Fourier-limited.⁶⁴ These signals were simulated for $\tau_{pu} = 5$ fs and $\tau_{pr} = 0$ fs (impulsive detection limit).

The integral signal excited with $\omega_{pu} = 4.03$ eV is shown in Figure 3. From left to right, the panels correspond to the GSB, SE, and ESA contributions and the total integral signal. From top to bottom, the panels correspond to the polarizations of the pump and probe pulses (ϵ_{pu} , ϵ_{pr}) along the axes (X–X), (X–Y), (Y–Y), and (Y–X) of the reference frame shown in Scheme 1.

When the central frequency of the pump pulse is resonant with S_1 , the excitation mainly brings the system into S_1 . The TDM from S_0 to S_1 is mainly along the X-axis: $\mu_{0,1}^x = 12.09$ D and $\mu_{0,1}^y = -1.36$ D (see Table 1). As a result, only the pump pulse with $\epsilon_{pu} \parallel X$ excites the S_1 state significantly.

Let us first consider the TA PP signal when the polarization of the probe pulse is also along the X-axis ($\epsilon_{pr} \parallel X$), as shown in Figure 3a. In Figure 3a-1, the GSB signal manifests electronic transitions between S_0 and S_1 , which exhibits low-amplitude oscillations around $\omega_{pr} \approx 4.0$ eV. Such oscillations reveal the high-frequency CC triple bond stretching mode with a period ~15 fs and are caused by the combination of non-Condon effects, anharmonic effects, and finite pulse duration.

The SE signal, which is shown in Figure 3a-2, gives important information on the excited-state wavepacket motion. After being pumped, the system remains on the S_1 potential energy surface (PES) according to the population dynamics in Figure 2a. In this case, the SE signal reflects the projection of the time-dependent excited-state wavepacket motion in the lowest excited electronic state to the electronic ground state. At $\tau = 0$, the maximum of the SE signal corresponds to $\omega_{pr} \approx 4.0$ eV. Then the “center of gravity” of the SE signal moves to the red and oscillates around ~3.5 eV, which is close to the VEE of the S_1 state at S_1 -min (see Table S2). Similar to the GSB signals, the oscillation of the SE signal is mainly due to the evolution of the S_1 VEE under the stretching vibration of the CC triple bonds (r_2 and r_3) at the 3-ring unit. As discussed above, the significant elongations of r_2 and r_3 take place from S_0 -min to S_1 -min (see Table S2). To clarify this argument, we examined the time-dependent evolution of the symmetric and asymmetric combinations of stretching vibrations of r_2 and r_3 and found that the symmetric stretching vibration (Figure S3d-2) gives the same oscillation patterns as the SE signal. This indicates that the symmetric stretching vibration of the CC triple bonds at the 3-ring unit drives the system to move forward and backward with respect to the geometry of S_1 -min, producing high-amplitude SE oscillations. No SE decay was observed in the whole simulation time, which is consistent with the fact that the system always stays on S_1 if the dynamics starts from S_1 (see Figure 2a).

The ESA signal is shown in Figure 3a-3. This signal reflects the projection of the wavepacket motion in the S_1 state to the high-lying excited states of manifold {II}. The ESA signal is centered at $\omega_{pr} \approx 1.7$ eV, which reveals the S_1 -to- S_{12} transition having a much larger TDM component in the X-axis direction than other {I} → {II} transitions (see Figure 1a-2). A low-amplitude ESA signal oscillation with a period of 15 fs reveals the same CC triple bond stretching. To clarify why the amplitude of this oscillation is rather low, we calculated the

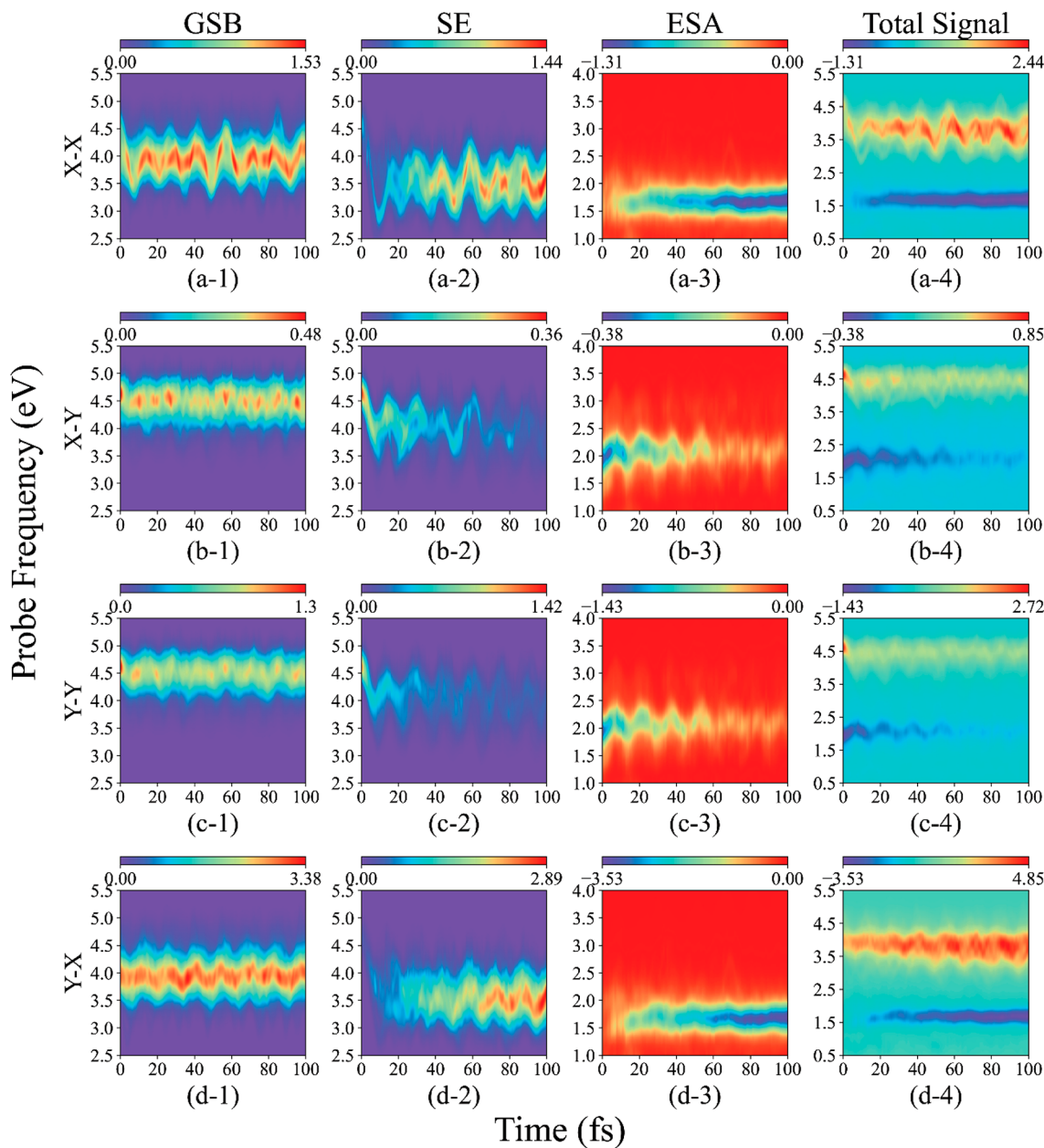


Figure 4. (1) GSB, (2) SE, and (3) ESA contributions and (4) total integral signal $I_{\text{int}}(\tau, \omega_{\text{pr}})$ as a function of τ and ω_{pr} . The notation $\alpha-\beta$ ($\alpha, \beta = X, Y$) on the left side indicates that the pump pulse polarization (ϵ_{pu}) is along the α -axis direction, while the probe pulse polarization (ϵ_{pr}) is along the β -axis direction. The central frequency of the pump pulse is $\omega_{\text{pu}} = 4.64$ eV, and the pulse durations are $\tau_{\text{pu}} = \tau_{\text{pr}} = 5$ fs.

excitation energies of several higher excited states along three CC triple bonds (r_1 , r_2 , and r_3). The electronic state with the largest x -component of TDM μ^x from S_1 is followed, and the corresponding transition energy is given in Figure S6. Clearly, the transition energy is weakly dependent on the oscillation range of r_2 and r_3 for the trajectories moving on the S_1 state (Figure S3), explaining the low-amplitude oscillation of the ESA signal in Figure 3a-3.

The total signal, which is the sum of the GSB, SE, and ESA contributions, is shown in Figure 3a-4. Although the GSB and SE signals show a little overlap, they can be easily distinguished from the ESA signal because the latter one is located in a different spectral domain. In this sense, this system is a promising candidate for the future experimental TA PP study because the ESA signal does not overlap with the GSB and SE signals.

Next, we will discuss the integral TA PP signal for $\epsilon_{\text{pu}}||X$ and $\epsilon_{\text{pr}}||Y$, which is shown in Figure 3b. As discussed above, the Y -component of the TDM from S_0 to S_2 , ($\mu_{0,2}^y = -5.97$ D) is almost four times larger than the Y -component of the TDM from S_0 to S_1 , ($\mu_{0,1}^y = -1.36$ D). Hence, the GSB signal (Figure 3b-1) is centered at $\omega_{\text{pr}} \approx 4.5$ eV, close to the VEE of S_2 in the FC region (see Table S2). Therefore, the GSB signal is dominated by the electronic transition to S_2 . Because $\mu_{0,1}^y < \mu_{0,1}^x$, the SE signal shown in Figure 3b-2 is much weaker than that in Figure 3a-2. Similar to the TA PP signals with $\epsilon_{\text{pr}}||X$, the oscillation of the present SE signal reflects the wavepacket motion in the S_1 state.

The ESA signal in Figure 3b-3 is due to the transitions from S_1 to several higher excited states, which are induced by the probe pulse with $\epsilon_{\text{pr}}||Y$. This signal differs considerably from its counterpart induced by the probe pulse with $\epsilon_{\text{pr}}||X$ shown in

Figure 3a-3. The reason is that the Y-components of the TDMs from S_1 to several higher excited states (S_4 , S_{24} , and S_{30}) are rather similar, as shown in **Figure 1b-2**. As a result, the ESA signal becomes diffuse in the probe frequency domain from 1.7 to 3.7 eV.

The total signal for the Y-polarized probe pulse is shown in **Figure 3b-4**, in which the GSB contribution dominates. At the same time, the GSB signal is well separated from the SE and ESA signals, while the late two components overlap with each other, resulting in the partial cancellation of the signal at 2.5–4.0 eV.

When the polarization of the pump pulse is along the Y-axis direction, namely, $\epsilon_{pu} \parallel Y$, as shown in **Figure 3c,d**, the signals become more complicated because S_2 is also involved in the Y-axis excitation. However, it is not worthwhile to discuss them in detail, because the intensities of these signals are much weaker than those with $\epsilon_{pu} \parallel X$.

It is necessary to point out that the intensity of the GSB, SE, and ESA contributions for $\epsilon_{pu} = \epsilon_{pr} \parallel X$ (**Figure 3a**) is much stronger than that for other combinations of the polarization vectors (**Figure 3b-d**) because of much weaker TDM components. Thus, the total TA PP signal is also dominated by the $X-X$ contribution depicted in **Figure 3a-4**.

The integral signal for $\omega_{pu} = 4.64$ eV is shown in **Figure 4**. In this case, the pump frequency is resonant with the $S_0 \rightarrow S_2$ transition. Here, the $S_0 \rightarrow S_2$ TDM has X- and Y-components of comparable intensity: $\mu_{0,2}^x = 2.88$ D and $\mu_{0,2}^y = -5.97$ D (see **Table 1**). Thus, TA PP signals have considerable intensity for any polarization of pump and probe pulses (**Figure 4a-d**). That is why the signals with $\epsilon_{pu} \parallel X$ and $\epsilon_{pu} \parallel Y$ are qualitatively similar. For the sake of simplicity, we focus on the analysis of the signals with $\epsilon_{pu} \parallel Y$ (**Figure 4c,d**) because of $\mu_{0,2}^y > \mu_{0,2}^x$.

According to eqs 18 and 19 in the **Supporting Information**, the GSB signal is always dominated by the strongest electronic transition caused by the probe pulse. The GSB signals in **Figure 4c-1,d-1** are dominated by the transitions to the states S_2 and S_1 , for $\epsilon_{pr} \parallel Y$ and $\epsilon_{pr} \parallel X$, respectively. As a result, the GSB signals in **Figure 4c-1,d-1** are very similar to those in **Figures 4b-1,a-1**. The minor difference is caused by slightly different doorway functions. In addition, the excitation of the S_2 state may also trigger the excitation of the S_3 state because of the small energy gap between the two states and relatively high spectral width of 5 fs pump and probe pulses. The SE signal in **Figure 4c-2** monitors the excited-state nonadiabatic dynamics initiated in the state S_2 . In the beginning, the SE maximum is located at $\omega_{pr} \approx 4.6$ eV, which is close to the VEE of the S_2 state in the FC region (**Table S2**). Then the wavepacket starts moving on the S_2 PES, and its motion is manifested through the oscillatory patterns of the SE signal. After a while, the wavepacket reaches the S_1/S_2 PES crossing and transfers to the S_1 state. Thus, the oscillatory SE signal becomes weaker with time and nearly disappears after 80 fs. The rapid quenching of the SE signal is consistent with the S_2 population dynamics shown in **Figure 2b**. Most importantly, while the SE signal for $\epsilon_{pr} \parallel Y$ decays (**Figure 4c-2**), the SE signal for $\epsilon_{pr} \parallel X$ rises (**Figure 4d-2**). The reason is that the SE signal for $\epsilon_{pr} \parallel Y$ originates mainly from the local excitation at the 2-ring unit, while the SE signal for $\epsilon_{pr} \parallel X$ is dominated by the local excitation at the 3-ring unit. Therefore, quenching of the SE signal in the Y direction and simultaneous rise of the SE signal in the X direction is a clear fingerprint of the ultrafast energy transfer from the 2-ring to the 3-ring unit.

The ESA signal for $\epsilon_{pr} \parallel Y$ is shown in **Figure 4c-3**. The signal reveals absorption from S_2 to other high-lying states of manifold {II} at the 2-ring unit. The signal is located around $\omega_{pr} \approx 2.0$ eV, which matches $S_2 \rightarrow S_{24}$ transition caused by the TDM that has the strongest component in the Y direction (see **Figure 1b-3**). Similar to the SE signal, the ESA signal exhibits a pronounced oscillatory pattern that reflects the nuclear motion on the S_2 PES. In addition, the ESA intensity in the Y direction decreases with time (**Figure 4c-3**) while the ESA intensity in the X direction increases (**Figure 4d-3**). This is another indication of the 2-ring to 3-ring energy transfer.

The total signals probed in the Y and X directions are shown in panels c-4 and d-4 of **Figure 4**, respectively. The mechanism and time scale of the excited-state energy-transfer process can clearly be deduced by combining these two signals. The clearest picture is obtained by examining the ESA signal that is well-separated from the GSB and SE signals: its vanishing in the Y direction and appearance in the X direction directly reflect the nonadiabatically driven excited-state energy transfer from the 2-ring unit to the 3-ring unit. In spite of the spectral overlap of the GSB and SE signals, we clearly monitor the same process because the GSB+SE signal in the Y (X) direction decreases (increases) with time. It should also be noted that the SE signals in the X and Y directions are located at different wavelengths. The SE signal decays in the higher-energy domain in the Y direction while growing in the lower-energy domain in the X direction. This observation also reveals the excited-state energy transfer. This indicates that high time and frequency resolution in conjunction with polarization-sensitive detection of TA PP signals allows us to scrutinize excited-state energy transfer in dendrimers. We thus suggest that polarization-sensitive pump–probe experiments give a direct real-time fingerprint of intramolecular excited-state energy transfer if the involved localized electronic states possess different energies and different TDM orientations.

In this work, we simulated the TA PP signals of the PE dendrimer model system by combining the on-the-fly non-adiabatic dynamics and the DW representation of nonlinear spectroscopy. We incorporated polarizations of laser fields into the DW representation and simulated integral and dispersed TA PP signals for different polarizations of the pump and probe pulses

We carefully analyzed total TA PP signals as well as the GSB, SE, and ESA contributions. When the pump pulse is resonant with the $S_0 \rightarrow S_1$ transition and polarization of the pump pulse coincides with the $S_0 \rightarrow S_1$ TDM direction (X-axis), S_1 is significantly populated and the excited-state wavepacket dynamics driven by the stretching vibrations of the CC triple bonds is manifested in the high-amplitude oscillation of the SE signal. This oscillatory contribution is also pronounced when the probe pulse is polarized along the X-axis. The GSB signal depends significantly on the polarization of the probe pulse because different excited states have different TDM orientations. The ESA signal is spectrally well-separated from the overlapping GSB/SE counterparts and, similar to the SE signal, exhibits vibrational oscillations revealing the CC triple bonds.

When the pump pulse is resonant with the $S_0 \rightarrow S_2$ transition, S_2 is significantly populated for any polarization of the pump pulse. Next, a fast (~40 fs) $S_2 \rightarrow S_1$ internal conversion takes place, which corresponds to the excited-state energy transfer from the 2-ring to 3-ring units. The $S_0 \rightarrow S_1$ TDM has a large component in the X-direction only, while the

$S_0 \rightarrow S_2$ TDM has comparable X and Y components. Therefore, the SE signal with the Y-polarized probe quenches while the SE signal with the X-axis polarized probe pulse rises. Similar information is encoded in the ESA signals. We thus conclude that the use of different pump–probe polarizations provides direct spectroscopic evidence of the energy transfer from the short-conjugated unit to the long-conjugated unit in dendrimers.

This work demonstrates that on-the-fly nonadiabatic dynamics simulation combined with the DW representation of nonlinear spectroscopy provides a promising approach to ab initio calculations of time-resolved TA PP spectra. In particular, this methodology gives a practical and numerically feasible tool to simulate time-resolved spectra of those polyatomic systems which exhibit nonadiabatic dynamics in low-lying excited electronic states. In addition, this work clearly indicates that polarization-sensitive detection of TA PP signals in conjunction with ab initio on-the-fly simulation of these signals may provide a direct way to explore ultrafast energy-transfer in optically bright excited states possessing different TDM orientations. We hope that this idea may encourage additional experimental studies of similar systems in the future.

ASSOCIATED CONTENT

Supporting Information

The Supporting Information is available free of charge at <https://pubs.acs.org/doi/10.1021/acs.jpcllett.1c02640>.

Theoretical descriptions of the polarization-sensitive TA PP spectroscopy in the DW representation, quasi-classical evaluation, computational details, frontier molecular orbital, VEEs and TDMs along the stretching of CC triple bonds, time-dependent distributions of CC triple bonds, TA PP dispersed signals, scan of the transition energy from S_1 to the high-lying excited state, and long-time (200 fs) TA PP integral signals ([PDF](#))

AUTHOR INFORMATION

Corresponding Author

Zhenggang Lan — SCNU Environmental Research Institute, Guangdong Provincial Key Laboratory of Chemical Pollution and Environmental Safety & MOE Key Laboratory of Environmental Theoretical Chemistry, South China Normal University, Guangzhou 510006, China; School of Environment, South China Normal University, Guangzhou 510006, China; Email: zhenggang.lan@m.scnu.edu.cn, zhenggang.lan@gmail.com

Authors

Deping Hu — SCNU Environmental Research Institute, Guangdong Provincial Key Laboratory of Chemical Pollution and Environmental Safety & MOE Key Laboratory of Environmental Theoretical Chemistry, South China Normal University, Guangzhou 510006, China; School of Environment, South China Normal University, Guangzhou 510006, China; [orcid.org/0000-0001-7161-1253](#)

Jiawei Peng — SCNU Environmental Research Institute, Guangdong Provincial Key Laboratory of Chemical Pollution and Environmental Safety & MOE Key Laboratory of Environmental Theoretical Chemistry, South China Normal University, Guangzhou 510006, China; School of Environment, South China Normal University, Guangzhou 510006, China

Lipeng Chen — Max Planck Institute for the Physics of Complex Systems, 01187 Dresden, Germany; [orcid.org/0000-0003-1415-4767](#)

Maxim F. Gelin — School of Sciences, Hangzhou Dianzi University, Hangzhou 310018, China; [orcid.org/0000-0003-3092-3343](#)

Complete contact information is available at: <https://pubs.acs.org/10.1021/acs.jpcllett.1c02640>

Notes

The authors declare no competing financial interest.

ACKNOWLEDGMENTS

This work is supported by NSFC projects (Nos. 21933011 and 21873112). The authors thank the Supercomputing Center, Computer Network Information Center, Chinese Academy of Sciences; National Supercomputing Center in Shenzhen for providing computational resources. M.F.G. acknowledges the support of Hangzhou Dianzi University through startup funding.

REFERENCES

- (1) Raychaudhuri, S.; Shapir, Y.; Chernyak, V. V.; Mukamel, S. Excitonic funneling in extended dendrimers with nonlinear and random potentials. *Phys. Rev. Lett.* **2000**, *85*, 282–285.
- (2) Freixas, V. M.; Ondarce-Alvarez, D.; Tretiak, S.; Makhov, D. V.; Shalashilin, D. V.; Fernandez-Alberti, S. Photoinduced non-adiabatic energy transfer pathways in dendrimer building blocks. *J. Chem. Phys.* **2019**, *150*, 124301.
- (3) Fernandez-Alberti, S.; Roitberg, A. E.; Kleiman, V. D.; Nelson, T.; Tretiak, S. Shishiodoshi unidirectional energy transfer mechanism in phenylene ethynylene dendrimers. *J. Chem. Phys.* **2012**, *137*, 22A526.
- (4) Atas, E.; Peng, Z.; Kleiman, V. D. Energy transfer in unsymmetrical phenylene ethynylene dendrimers. *J. Phys. Chem. B* **2005**, *109*, 13553–13560.
- (5) Tortschanoff, A.; Mukamel, S. Pump-probe simulation study of the two-exciton manifold of dendrimers. *J. Phys. Chem. A* **2002**, *106*, 7521–7529.
- (6) Tretiak, S.; Mukamel, S. Density matrix analysis and simulation of electronic excitations in conjugated and aggregated molecules. *Chem. Rev.* **2002**, *102*, 3171–3212.
- (7) Nelson, T.; Fernandez-Alberti, S.; Roitberg, A. E.; Tretiak, S. Nonadiabatic excited-state molecular dynamics: Modeling photo-physics in organic conjugated materials. *Acc. Chem. Res.* **2014**, *47*, 1155–1164.
- (8) Kilina, S.; Kilin, D.; Tretiak, S. Light-driven and phonon-assisted dynamics in organic and semiconductor nanostructures. *Chem. Rev.* **2015**, *115*, 5929–5978.
- (9) Nelson, T. R.; White, A. J.; Bjorgaard, J. A.; Sifain, A. E.; Zhang, Y.; Nebgen, B.; Fernandez-Alberti, S.; Mozyrsky, D.; Roitberg, A. E.; Tretiak, S. Non-adiabatic excited-state molecular dynamics: Theory and applications for modeling photophysics in extended molecular materials. *Chem. Rev.* **2020**, *120*, 2215–2287.
- (10) Kirkwood, J. C.; Scheurer, C.; Chernyak, V.; Mukamel, S. Simulations of energy funneling and time- and frequency-gated fluorescence in dendrimers. *J. Chem. Phys.* **2001**, *114*, 2419–2429.
- (11) Fernandez-Alberti, S.; Kleiman, V. D.; Tretiak, S.; Roitberg, A. E. Nonadiabatic molecular dynamics simulations of the energy transfer between building blocks in a phenylene ethynylene dendrimer. *J. Phys. Chem. A* **2009**, *113*, 7535–7542.
- (12) Tada, T.; Nozaki, D.; Kondo, M.; Yoshizawa, K. Molecular orbital interactions in the nanostar dendrimer. *J. Phys. Chem. B* **2003**, *107*, 14204–14210.

- (13) Huang, J.; Du, L.; Hu, D.; Lan, Z. Theoretical analysis of excited states and energy transfer mechanism in conjugated dendrimers. *J. Comput. Chem.* **2015**, *36*, 151–163.
- (14) Fernandez-Alberti, S.; Makhov, D. V.; Tretiak, S.; Shalashilin, D. V. Non-adiabatic excited state molecular dynamics of phenylene ethynylene dendrimer using a multiconfigurational Ehrenfest approach. *Phys. Chem. Chem. Phys.* **2016**, *18*, 10028–10040.
- (15) Ondarse-Alvarez, D.; Kömürlü, S.; Roitberg, A. E.; Pierdominici-Sottile, G.; Tretiak, S.; Fernandez-Alberti, S.; Kleiman, V. D. Ultrafast electronic energy relaxation in a conjugated dendrimer leading to inter-branch energy redistribution. *Phys. Chem. Chem. Phys.* **2016**, *18*, 25080–25089.
- (16) Shortreed, M. R.; Swallen, S. F.; Shi, Z. Y.; Tan, W. H.; Xu, Z. F.; Devadoss, C.; Moore, J. S.; Kopelman, R. Directed energy transfer funnels in dendrimeric antenna supermolecules. *J. Phys. Chem. B* **1997**, *101*, 6318–6322.
- (17) Galindo, J. F.; Atas, E.; Altan, A.; Kuroda, D. G.; Fernandez-Alberti, S.; Tretiak, S.; Roitberg, A. E.; Kleiman, V. D. Dynamics of energy transfer in a conjugated dendrimer driven by ultrafast localization of excitations. *J. Am. Chem. Soc.* **2015**, *137*, 11637–11644.
- (18) Tretiak, S.; Chernyak, V.; Mukamel, S. Localized electronic excitations in phenylacetylene dendrimers. *J. Phys. Chem. B* **1998**, *102*, 3310–3315.
- (19) Alfonso Hernandez, L.; Nelson, T.; Gelin, M. F.; Lupton, J. M.; Tretiak, S.; Fernandez-Alberti, S. Interference of interchromophoric energy-transfer pathways in π -conjugated macrocycles. *J. Phys. Chem. Lett.* **2016**, *7*, 4936–4944.
- (20) Conti, I.; Cerullo, G.; Nenov, A.; Garavelli, M. Ultrafast spectroscopy of photoactive molecular systems from first principles: Where we stand today and where we are going. *J. Am. Chem. Soc.* **2020**, *142*, 16117–16139.
- (21) Hudock, H. R.; Martínez, T. J. Excited-state dynamics of cytosine reveal multiple intrinsic subpicosecond pathways. *Chem-PhysChem* **2008**, *9*, 2486–2490.
- (22) Bonačić-Koutecký, V.; Mitić, R. Theoretical Exploration of Ultrafast Dynamics in Atomic Clusters: Analysis and Control†. *Chem. Rev.* **2005**, *105*, 11–66.
- (23) Cusati, T.; Granucci, G.; Persico, M. Photodynamics and time-resolved fluorescence of azobenzene in solution: A mixed quantum-classical simulation. *J. Am. Chem. Soc.* **2011**, *133*, 5109–5123.
- (24) Klaumunzer, B.; Kroner, D.; Lischka, H.; Saalfrank, P. Non-adiabatic excited state dynamics of riboflavin after photoexcitation. *Phys. Chem. Chem. Phys.* **2012**, *14*, 8693–8702.
- (25) Lan, Z.; Lu, Y.; Weingart, O.; Thiel, W. Nonadiabatic decay dynamics of a benzylidene malononitrile. *J. Phys. Chem. A* **2012**, *116*, 1510–1518.
- (26) Pang, X. J.; Cui, X. Y.; Hu, D. P.; Jiang, C. W.; Zhao, D.; Lan, Z. G.; Li, F. L. "Watching" the dark state in ultrafast nonadiabatic photoisomerization process of a light-driven molecular rotary motor. *J. Phys. Chem. A* **2017**, *121*, 1240–1249.
- (27) Roy, S.; Ardo, S.; Furche, F. S-Methoxyquinoline Photobasicity Is Mediated by Water Oxidation. *J. Phys. Chem. A* **2019**, *123*, 6645–6651.
- (28) Yu, J. K.; Liang, R. B.; Liu, F.; Martinez, T. J. First-Principles Characterization of the Elusive I Fluorescent State and the Structural Evolution of Retinal Protonated Schiff Base in Bacteriorhodopsin. *J. Am. Chem. Soc.* **2019**, *141*, 18193–18203.
- (29) Polli, D.; Altoe, P.; Weingart, O.; Spillane, K. M.; Manzoni, C.; Brida, D.; Tomasello, G.; Orlandi, G.; Kukura, P.; Mathies, R. A.; et al. Conical intersection dynamics of the primary photoisomerization event in vision. *Nature* **2010**, *467*, 440–443.
- (30) Nenov, A.; Borrego-Varillas, R.; Oriana, A.; Ganzer, L.; Segatta, F.; Conti, I.; Segarra-Martí, J.; Omachi, J.; Dapor, M.; Taioli, S.; et al. UV-light-induced vibrational coherences: The key to understand Kasha rule violation in trans-Azobenzene. *J. Phys. Chem. Lett.* **2018**, *9*, 1534–1541.
- (31) Borrego-Varillas, R.; Teles-Ferreira, D. C.; Nenov, A.; Conti, I.; Ganzer, L.; Manzoni, C.; Garavelli, M.; Maria de Paula, A.; Cerullo, G. Observation of the sub-100 fs population of a dark state in a thiobase mediating intersystem crossing. *J. Am. Chem. Soc.* **2018**, *140*, 16087–16093.
- (32) Picchiotti, A.; Nenov, A.; Giussani, A.; Prokhortenko, V. I.; Miller, R. J. D.; Mukamel, S.; Garavelli, M. Pyrene, a test case for deep-ultraviolet molecular photophysics. *J. Phys. Chem. Lett.* **2019**, *10*, 3481–3487.
- (33) Nguyen, T. S.; Koh, J. H.; Lefelhocz, S.; Parkhill, J. Black-box, real-time simulations of transient absorption spectroscopy. *J. Phys. Chem. Lett.* **2016**, *7*, 1590–1595.
- (34) Bonafé, F. P.; Hernández, F. J.; Aradi, B.; Frauenheim, T.; Sánchez, C. G. Fully atomistic real-time simulations of transient absorption spectroscopy. *J. Phys. Chem. Lett.* **2018**, *9*, 4355–4359.
- (35) Krumland, J.; Valencia, A. M.; Pittalis, S.; Rozzi, C. A.; Cocchi, C. Understanding real-time time-dependent density-functional theory simulations of ultrafast laser-induced dynamics in organic molecules. *J. Chem. Phys.* **2020**, *153*, No. 054106.
- (36) Zimmermann, T.; Vaníček, J. Efficient on-the-fly ab initio semiclassical method for computing time-resolved nonadiabatic electronic spectra with surface hopping or Ehrenfest dynamics. *J. Chem. Phys.* **2014**, *141*, 134102.
- (37) Begušić, T.; Roulet, J.; Vaníček, J. On-the-fly ab initio semiclassical evaluation of time-resolved electronic spectra. *J. Chem. Phys.* **2018**, *149*, 244115.
- (38) Tancogne-Dejean, N.; Oliveira, M. J. T.; Andrade, X.; Appel, H.; Borca, C. H.; Le Breton, G.; Buchholz, F.; Castro, A.; Corni, S.; Correa, A. A.; et al. Octopus, a computational framework for exploring light-driven phenomena and quantum dynamics in extended and finite systems. *J. Chem. Phys.* **2020**, *152*, 124119.
- (39) Gelin, M. F.; Huang, X.; Xie, W.; Chen, L.; Doslic, N. A.; Domcke, W. Ab initio surface-hopping simulation of femtosecond transient-absorption pump-probe signals of nonadiabatic excited-state dynamics using the doorway-window representation. *J. Chem. Theory Comput.* **2021**, *17*, 2394–2408.
- (40) Yan, Y. J.; Fried, L. E.; Mukamel, S. Ultrafast pump-probe spectroscopy: femtosecond dynamics in Liouville space. *J. Phys. Chem.* **1989**, *93*, 8149–8162.
- (41) Yan, Y. J.; Mukamel, S. Femtosecond pump-probe spectroscopy of polyatomic molecules in condensed phases. *Phys. Rev. A: At., Mol., Opt. Phys.* **1990**, *41*, 6485–6504.
- (42) Fried, L. E.; Mukamel, S. A classical theory of pump–probe photodissociation for arbitrary pulse durations. *J. Chem. Phys.* **1990**, *93*, 3063–3071.
- (43) Hochstrasser, R. M. Two-dimensional IR-spectroscopy: polarization anisotropy effects. *Chem. Phys.* **2001**, *266*, 273–284.
- (44) Tan, H. S.; Piletic, I. R.; Fayer, M. D. Polarization selective spectroscopy experiments: methodology and pitfalls. *J. Opt. Soc. Am. B* **2005**, *22*, 2009–2017.
- (45) Zanni, M. T.; Ge, N. H.; Kim, Y. S.; Hochstrasser, R. M. Two-dimensional IR spectroscopy can be designed to eliminate the diagonal peaks and expose only the crosspeaks needed for structure determination. *Proc. Natl. Acad. Sci. U. S. A.* **2001**, *98*, 11265–11270.
- (46) Gelin, M. F.; Domcke, W. Simple recipes for separating excited-state absorption and cascading signals by polarization-sensitive measurements. *J. Phys. Chem. A* **2013**, *117*, 11509–11513.
- (47) Varnavski, O. P.; Ostrowski, J. C.; Sukhomlinova, L.; Twieg, R. J.; Bazan, G. C.; Goodson, T. Coherent effects in energy transport in model dendritic structures investigated by ultrafast fluorescence anisotropy spectroscopy. *J. Am. Chem. Soc.* **2002**, *124*, 1736–1743.
- (48) Becker, K.; Fritzsche, M.; Höger, S.; Lupton, J. M. Phenylene–ethynylene macrocycles as model systems of interchromophoric interactions in π -conjugated macromolecules. *J. Phys. Chem. B* **2008**, *112*, 4849–4853.
- (49) Tully, J. C. Molecular dynamics with electronic transitions. *J. Chem. Phys.* **1990**, *93*, 1061–1071.
- (50) Wang, L. J.; Akimov, A.; Prezhdo, O. V. Recent progress in surface hopping: 2011–2015. *J. Phys. Chem. Lett.* **2016**, *7*, 2100–2112.

- (51) Crespo-Otero, R.; Barbatti, M. Recent advances and perspectives on nonadiabatic mixed quantum-classical dynamics. *Chem. Rev.* **2018**, *118*, 7026–7068.
- (52) Mai, S.; Marquetand, P.; González, L. Nonadiabatic dynamics: The SHARC approach. *Wiley Interdiscip. Rev.: Comput. Mol. Sci.* **2018**, *8*, No. e1370.
- (53) Persico, M.; Granucci, G. An overview of nonadiabatic dynamics simulations methods, with focus on the direct approach versus the fitting of potential energy surfaces. *Theor. Chem. Acc.* **2014**, *133*, 1526.
- (54) Curchod, B. F. E.; Martínez, T. J. Ab initio nonadiabatic quantum molecular dynamics. *Chem. Rev.* **2018**, *118*, 3305–3336.
- (55) Barbatti, M.; Granucci, G.; Persico, M.; Ruckenbauer, M.; Vazdar, M.; Eckert-Maksić, M.; Lischka, H. The on-the-fly surface-hopping program system NEWTON-X: Application to ab initio simulation of the nonadiabatic photodynamics of benchmark systems. *J. Photochem. Photobiol., A* **2007**, *190*, 228–240.
- (56) Aleotti, F.; Soprani, L.; Nenov, A.; Berardi, R.; Arcioni, A.; Zannoni, C.; Garavelli, M. Multidimensional potential energy surfaces resolved at the RASPT2 level for accurate photoinduced isomerization dynamics of azobenzene. *J. Chem. Theory Comput.* **2019**, *15*, 6813–6823.
- (57) Hu, D.; Liu, Y. F.; Sobolewski, A. L.; Lan, Z. Nonadiabatic dynamics simulation of keto isocytosine: a comparison of dynamical performance of different electronic-structure methods. *Phys. Chem. Chem. Phys.* **2017**, *19*, 19168–19177.
- (58) Du, L. K.; Lan, Z. G. An on-the-fly surface-hopping program JADE for nonadiabatic molecular dynamics of polyatomic systems: Implementation and applications. *J. Chem. Theory Comput.* **2015**, *11*, 1360–1374.
- (59) Frisch, M. J.; Trucks, G. W.; Schlegel, H. B.; Scuseria, G. E.; Robb, M. A.; Cheeseman, J. R.; Scalmani, G.; Barone, V.; Petersson, G. A.; Nakatsuji, H., et al. *Gaussian 16*, Rev. C.01; Wallingford, CT, 2016.
- (60) Shao, Y.; Gan, Z.; Epifanovsky, E.; Gilbert, A. T. B.; Wormit, M.; Kussmann, J.; Lange, A. W.; Behn, A.; Deng, J.; Feng, X.; et al. Advances in molecular quantum chemistry contained in the Q-Chem. 4 program package. *Mol. Phys.* **2015**, *113*, 184–215.
- (61) Zhang, X.; Herbert, J. M. Analytic derivative couplings for spin-flip configuration interaction singles and spin-flip time-dependent density functional theory. *J. Chem. Phys.* **2014**, *141*, No. 064104.
- (62) Ou, Q.; Fatehi, S.; Alguire, E.; Shao, Y.; Subotnik, J. E. Derivative couplings between TDDFT excited states obtained by direct differentiation in the Tamm-Dancoff approximation. *J. Chem. Phys.* **2014**, *141*, No. 024114.
- (63) Malone, W.; Nebgen, B.; White, A.; Zhang, Y.; Song, H.; Bjorgaard, J. A.; Sifain, A. E.; Rodriguez-Hernandez, B.; Freixas, V. M.; Fernandez-Alberti, S.; et al. NEXMD software package for nonadiabatic excited state molecular dynamics simulations. *J. Chem. Theory Comput.* **2020**, *16*, 5771–5783.
- (64) Palacino-González, E.; Gelin, M. F.; Domcke, W. Analysis of transient-absorption pump-probe signals of nonadiabatic dissipative systems: “Ideal” and “real” spectra. *J. Chem. Phys.* **2019**, *150*, 204102.